Microenvironmental mechanoactivation through Yap/Taz suppresses chondrogenic gene expression

Grey F. Hallström[a,b,c], Dakota L. Jones[a], Ryan C. Locke[a,b,c], Edward D. Bonnevie[a,b,c], Sung Yeon Kim[a,b,c,d], Lorielle Laforest[a], Diana Cruz Garcia[a], and Robert L. Mauck[a,b,c,d,*]

[a]McKay Orthopaedic Research Laboratory, Department of Orthopaedic Surgery, Perelman School of Medicine; [b]Center for Engineering Mechanobiology, and [d]Department of Bioengineering, School of Engineering and Applied Science, University of Pennsylvania, Philadelphia, PA 19104; [c]Translational Musculoskeletal Research Center, Corporal Michael J. Crescenz VA Medical Center, Philadelphia, PA 19104

ABSTRACT **Chondrocyte phenotype is preserved when cells are round and the actin cytoskeleton is cortical. Conversely, these cells rapidly dedifferentiate in vitro with increased mechanoactive Rho signaling, which increases cell size and causes large actin stress fiber to form. While the effects of Rho on chondrocyte phenotype are well established, the molecular mechanism is not yet fully elucidated. Yap, a transcriptional coregulator, is regulated by Rho in a mechanotransductive manner and can suppress chondrogenesis in vivo. Here, we sought to elucidate the relationship between mechanoactive Rho and Yap on chondrogenic gene expression. We first show that decreasing mechanoactive state through Rho inhibition results in a broad increase in chondrogenic gene expression. Next, we show that Yap and its coregulator Taz are negative regulators of chondrogenic gene expression, and removal of these factors promotes chondrogenesis even in environments that promote cell spreading. Finally, we establish that Yap/Taz is essential for translating Rho-mediated signals to negatively regulate chondrogenic gene expression, and that its removal negates the effects of increased Rho signaling. Together, these data indicate that Rho is a mechanoregulator of chondrogenic differentiation, and that its impact on chondrogenic expression is exerted principally through mechanically induced translocation and activity of Yap and Taz.**

Monitoring Editor
Michael Murrell
Yale University

Received: Dec 9, 2022
Revised: Mar 23, 2023
Accepted: Apr 6, 2023

This article was published online ahead of print in MBoC in Press (http://www.molbiolcell.org/cgi/doi/10.1091/mbc.E22-12-0543) on April 12, 2023.

Author contributions: G.F.H. and R.L.M. conceptualized the research goals and aims; G.F.H. curated the data; G.F.H., D.L.J., R.C.L., E.D.B., S.Y.K., L.L., and D.C.G. performed the formal analysis; R.L.M. acquired the funding for the research project; G.F.H. conducted the research in this investigation; G.F.H., D.L.J., R.C.L., E.D.B., and S.Y.K. developed the methodology for this study; G.F.H. and R.L.M. managed the project administration; R.L.M. and D.L.J. provided resources to complete this study; G.F.H., D.L.J., R.C.L., E.D.B., and S.Y.K. provided software needed to analyze the data acquired; R.L.M. supervised the study; G.F.H. validated the results generated in this study; G.F.H. and L.L. performed the visualization of the data presented in this study; G.F.H. wrote the original draft; all authors helped to review and edit the paper.

*Address correspondence to: Robert L. Mauck (lemauck@pennmedicine.upenn.edu).

Abbreviations used Acan, Aggrecan; BM, basal media; C3, C3 transferase; CM, chondrogenic media; ECM, extracellular matrix; LPA, 1-oleoyl lysophosphatidic acid; MMP, matrix metalloproteinases; PCM, pericellular matrix; Y/T, Yap/Taz.

INTRODUCTION

Articular cartilage is a mechanoadaptive tissue. Chondrocytes, the cells within cartilage, transduce dynamic physiologic forces to regulate expression of key matrix molecules, increasing anabolic production with physiologic loading and catabolic production with supraphysiologic and/or injurious loads (Sophia Fox *et al*., 2009; Sanchez-Adams *et al*., 2014). While this establishes that chondrocytes are mechanosensors that interpret the loading environment to regulate tissue homeostasis and degeneration, the molecular mechanism by which chondrocytes respond to their changing physical microenvironment, or mechanotransduce, remains an open question.

Mechanotransduction is the process by which cells convert mechanical stimuli into a biochemical response, such as changes to cytoskeletal architecture, focal adhesion formation, and/or changes in transcription factor activity (Dupont *et al*., 2011; Driscoll *et al*., 2015; Elosegui-Artola *et al*., 2017). Mechanotransductive inputs may include changes in substrate stiffness, dimensionality, mechanical loading, and/or cell shape with these inputs transmitted, in part, through the cytoskeleton (Gao *et al*., 2010; Dupont *et al*., 2011;

Heo *et al.*, 2015; Caliari *et al.*, 2016). Cytoskeletal-nuclear mechanotransduction utilizes connections between the actin cytoskeleton and the linker of nucleoskeletal and cytoskeletal (LINC) complex to mechanically couple the nucleus to its microenvironment (Luxton *et al.*, 2011; Driscoll *et al.*, 2015; Carley *et al.*, 2021). For example, one well-defined pathway involves Rho activation promoting F-actin fiber (stress fibers) formation, which in turn promotes the transcriptional coregulator Yap and its transcriptional coregulator Taz to translocate to the nucleus in response to mechanotransductive signals (Xu *et al.*, 2012; Das *et al.*, 2016). Increased Yap nuclear localization is due, in part, to increased nuclear strain (wrought by increased actin tension), which in turn increases nuclear pore permeability (Elosegui-Artola *et al.*, 2017). These pathways have been well established in fibroblasts and other cell types in 2D culture, but how these pathways operate in chondrocytes to regulate chondrogenic phenotype remains underexplored.

Seminal studies using primary chondrocytes show that the actin cytoskeleton and Rho play an important role in chondrocyte homeostasis and differentiation. Developing chondrocytes in the limb bud change their morphology from an elongated to a spherical shape (Barna and Niswander, 2007; Ray and Chapman, 2015; Decker *et al.*, 2017). This spherical cell shape is maintained, in part, by the actin cytoskeleton, which is arranged into a cortical network underlying the plasma membrane and is maintained in fully differentiated chondrocytes (Barna and Niswander, 2007; Blain, 2009). However, chondrocytes cultured in monolayer, typically on a supraphysiologic substrate such as tissue culture plastic, remodel their actin cytoskeleton toward a stress fiber–dominant cytoarchitecture (Woods *et al.*, 2005; Kumar and Lassar, 2009). This increased stress fiber formation correlates with a reduction in chondrocyte phenotype, including reduced expression of chondrogenic markers (Sox9, Col2a1, Aggrecan). Notably, the loss of chondrocyte phenotype can be rescued when stress fibers are disrupted (via pharmacologic inhibition or return to 3D culture; Woods *et al.*, 2005; Kumar and Lassar, 2009). Similarly, if Rho/ROCK signaling is directly increased, chondrocyte phenotype decreases along with formation of stress fibers. This suggests that Rho/ROCK is a central regulator of chondrogenic differentiation. Of note, when effectors of Rho/ROCK signaling are increased through genetic manipulation in vivo (i.e., YAP activation), cartilage formation and early chondrogenic marker gene expression is curtailed (Deng *et al.*, 2016; Öztürk *et al.*, 2017; Vanyai *et al.*, 2020). However, the direct link between effects of Yap on chondrogenic gene expression downstream from changes in actin and Rho/ROCK signaling has not yet been established.

Given the inverse relationship between elevated Rho signaling and chondrogenic gene expression, as well as recent data implicating Yap in cartilage development, we hypothesized that RhoA/ROCK signaling through Yap negatively regulates chondrogenic gene expression. Although aspects of this pathway have been shown to be important in cartilage, the precise relationship and centrality of Yap/Taz in chondrocyte interpretation of mechanical cues has not been fully delineated. To address this knowledge gap, we used ATDC5 cells, a chondroprogenitor cell line, cultured under chondrogenic conditions. These cells were challenged with small molecules and changes in microenvironmental stiffness to regulate Rho/ROCK activation, both in the presence and in the absence of Yap (and Taz). Using both canonical chondrogenic markers and broad evaluation of phenotype by RNA-seq, we show that Rho is a mechanoregulator of chondrogenic differentiation, and that its impact on chondrogenic expression is exerted principally through mechanically induced translocation and activity of Yap and Taz. These data provide new insight into mechanical regulation of the chondrocyte phenotype and may be leveraged to promote therapeutic cell expansion and design improved regenerative strategies.

RESULTS

To establish that ATDC5 cells respond to both Rho inhibition and activation when cultured in a robust chondrogenic differentiation media (CM; Supplemental Figure S1A), C3 transferase (C3) was used to inhibit Rho activity while 1-oleoyl lysophosphatidic acid (LPA) was used to promote Rho activity. Cells were first cultured in a high-density monolayer to maximally stimulate chondrogenic differentiation for 3 d in the presence or absence of C3 or LPA, and canonical markers of chondrogenesis were assayed. Changes in expression of these markers, *Sox9*, *Col2a1*, and Aggrecan (*Acan*) were used to assess differentiation status here, and for all subsequent studies. After 3 d of Rho inhibition with C3, a significant increase in all chondrogenic markers was observed in comparison to controls (Supplemental Figure S1B). Conversely, at this same time point, LPA treatment (to increase Rho activity) decreased chondrogenic marker gene expression (Supplemental Figure S1B). This was also verified at the protein level, where C3 generally increased total SOX9 protein levels over time (reaching significance at day 1 and 8 d; Supplemental Figure S2A). Consistent with previous literature, these data establish that modulation of Rho signaling impacts chondrogenic gene expression (Woods *et al.*, 2005). However, these canonical markers represent only a portion of the full chondrocyte phenotype.

To develop a more comprehensive view of the global transcriptomic changes that accompany Rho inhibition and activation, ATDC5 cells were treated with C3 or LPA for 3 d in high-density monolayer followed by evaluation by RNA-seq. With Rho inhibition, several chondrogenic genes not previously described as responsive to changes in Rho signaling emerged as significantly up-regulated, including *Gdf5*, *Nkx3-2*, *Col6a1-3*, *Col9a2*, and *Col11a1* (Figure 1A, highlighted points in volcano plot, i, and heatmap, ii). Notably, *Gdf5* and *Col6* and are important for articular cartilage formation and regulating articular chondrocyte mechanotransduction, respectively (Koyama *et al.*, 2008; Zelenski *et al.*, 2015), and both IF and Western blotting confirmed an increase in COLVI protein production with C3 (Figure 1, C and D, and Supplemental Figure S2B). Gene ontology (GO) analysis showed that for Rho inhibition, markers associated with positive regulation of chondrocyte differentiation were present in the modulated data set (Figure 1A, iii). LPA treatment, on the other hand, led to a significant increase in several catabolic extracellular matrix (ECM) proteins, including matrix metalloproteinases (MMPs) –3, –9, –10, –12, and –13 (Figure 1B, highlighted points in volcano plot, i, and heatmap, ii; Mehana *et al.*, 2019). The top GO terms in this context included collagen catabolic processes, ossification, ECM disassembly, endochondral ossification, and nitric oxide support (Figure 1B, iii). The full set of genes differentially regulated between C3 and LPA treatment are provided as Supplemental Material. These results demonstrate that, in the context of a prochondrogenic chemical environment, inhibition of Rho drives fate commitment toward the chondrocyte lineage while activating Rho signaling promotes a more matrix remodeling/proosteogenic transformation.

To assess whether Rho activity mediated changes in phenotype correlate with the mechanobiologic state of cells following C3 or LPA treatment, cells were seeded at low density on glass, given that Yap nuclear localization in the absence of cell–cell contacts is mediated by mechanotransductive-related pathways (i.e., Rho; Das *et al.*, 2016). Cell and nuclear area and Yap nuclear localization were

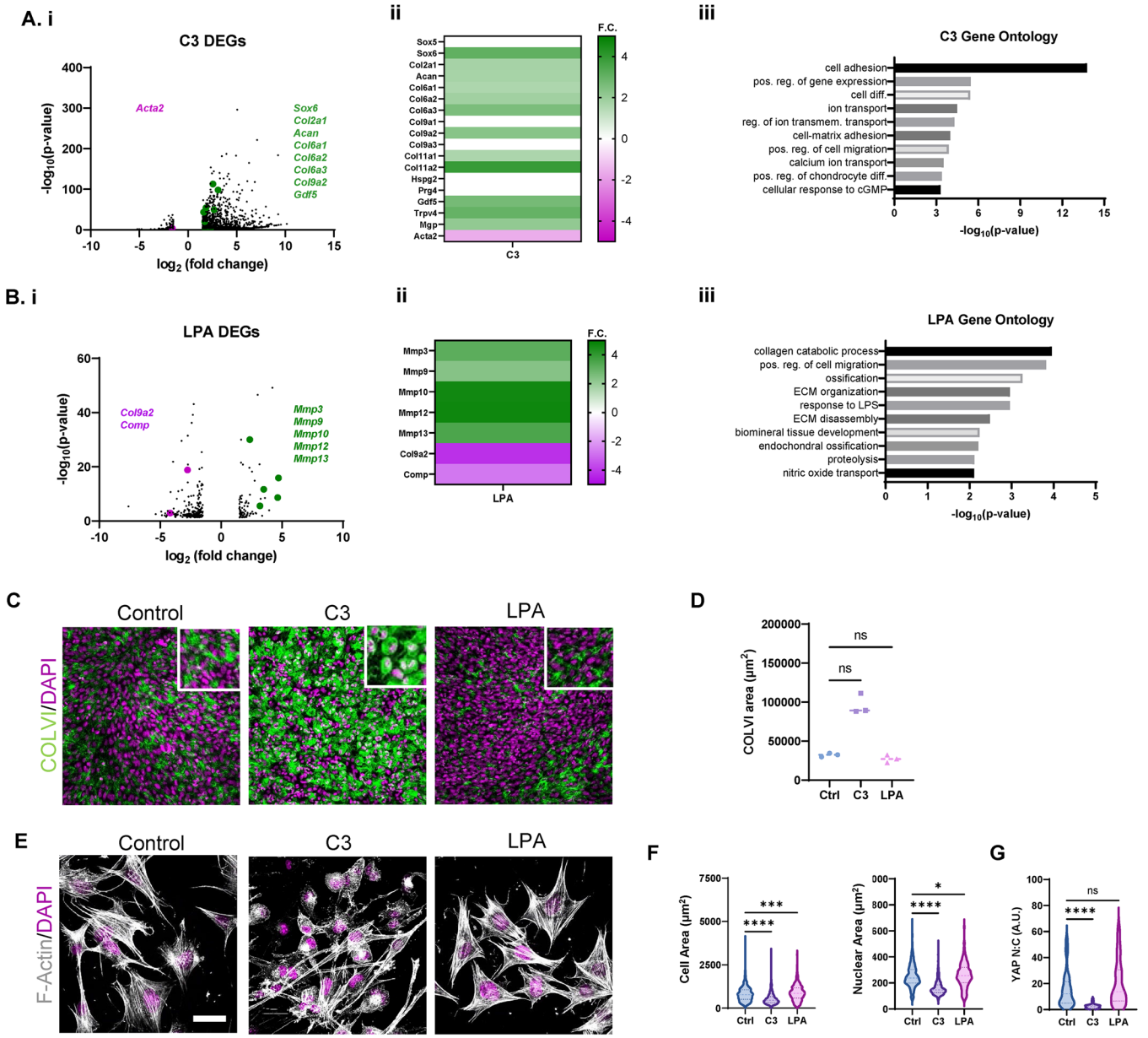

FIGURE 1: Rho inhibition drives a broad chondrogenic program and decreases YAP and TAZ nuclear localization. (A, i) Volcano plot showing differentially expressed genes (DEGs) following high-density culture with C3 treatment for 3 d in CM, relative to untreated controls. Genes showing significant differences have an established role in chondrocyte differentiation (chartreuse dots) or disease (magenta dots). (A, ii) Heatmap of noted genes in i. (A, iii) Bar graphs showing gene ontology groups identified from DEGs in i, in descending order of significance. $n = 3$ independent trials. (B, i) Volcano plot showing DEGs following high-density culture with LPA treatment for 3 d in CM, relative to untreated controls. Genes showing significant differences (chartreuse and magenta dots) have an established role in chondrocyte differentiation or disease. (A, ii) Heatmap of genes in i. (A, iii) Bar graphs showing gene ontology groups identified from DEGs in i, in descending order of significance. $n = 3$ independent trials. (C) Immunostaining of COLVI showing changes in organization and deposition amount. Nuclei were stained with DAPI. Maximum projection z-stack confocal images shown are representative images after 5 d of high-density culture with C3 or LPA treatment in CM. $n = 3$ independent trials. Scale bar = 100 μm. (D) Quantification of COLVI area signal from C. (E) F-actin immunostaining after 3 d in low-density culture with C3 or LPA treatment. Maximum projection z-stack confocal images. Scale bar = 30 μm. (F) Quantification of cell and nuclear area for cells treated with C3 or LPA in CM. (G) Quantification of YAP nuclear:cytoplasmic ratio (YAP N:C) for cells treated with C3 or LPA (right). $n = 3$ replicates, 20–30 cells per group/per replicate (*, $p < 0.05$; **, $p < 0.01$; ***, $p < 0.001$; ****, $p < 0.0001$).

assessed via immunostaining. C3 treatment decreased the presence of stress fibers while promoting a more punctate cortical actin. Conversely, LPA treatment resulted in a slight increase in actin stress fibers (albeit small given that the cells were already on a stiff substrate; Figure 1E). These changes in cytoarchitecture resulted in quantitative changes in cell morphology. Specifically, C3 treatment decreased cell and nuclear area while LPA treatment increased cell and nuclear area (Figure 1F). Given the close association between

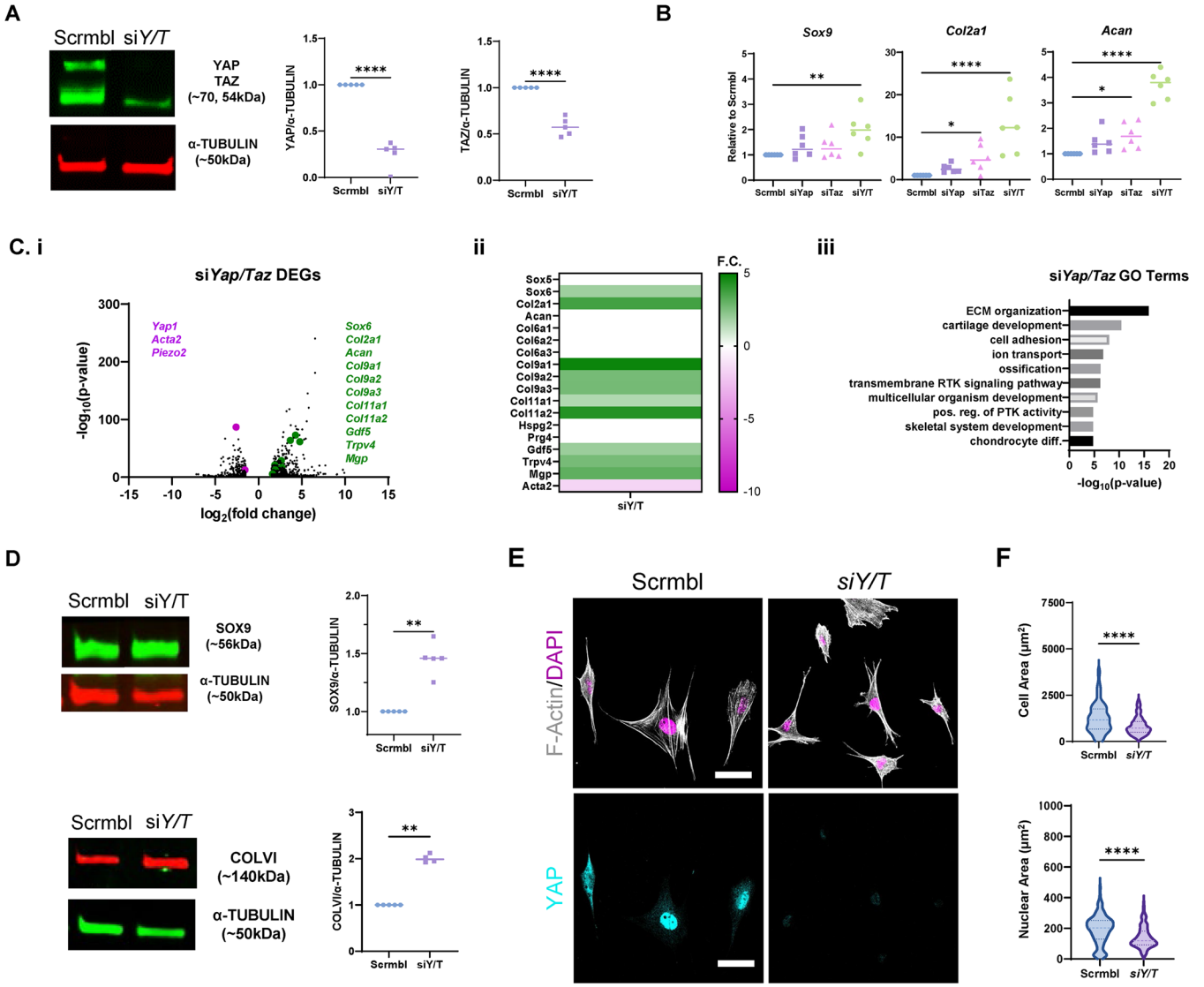

FIGURE 2: Yap/Taz act downstream from Rho to negatively regulate the chondrogenic program. (A) Immunoblot of Yap/Taz following siY/T transfection in CM. α-Tubulin was used as a loading control. $n = 5$ independent trials. (B) Chondrogenic gene expression of cells transfected with si*Yap1*, si*Taz*, or si*Y/T* in CM. $n = 6$ independent trials. (C, i) Volcano plot showing differentially expressed genes (DEGs) after siY/T transfection in CM, compared with nontargeting control (Scrmbl). Genes with significant differences in expression levels that have an established role in chondrocyte differentiation (chartreuse dots) or disease (magenta dots). (C, ii) Heatmap of noted genes in i. (C, iii) Bar graphs showing gene ontology groups identified from DEGs in i, in descending order of significance. $n = 3$ independent trials. (D) Left, SOX9 and COLVI immunoblot 5 d posttransfection with si*Y/T* in CM. Right, quantification of fold change in protein. $n = 5$ independent trials. α-Tubulin was used as a loading control. (E) F-actin and YAP immunostaining in cells transfected with nontargeting control (Scrmbl) or siY/T and cultured in low density at day 5 in CM. $n = 3$ independent trials. Maximum projection z-stack confocal images. Scale bar = 30 um. (F) Quantification of cell and nuclear area for cells transfected with Scrmbl or si*Y/T* (*, $p < 0.05$; **, $p < 0.01$; ***, $p < 0.001$; ****, $p < 0.0001$).

cell morphology and mechanical activation, we next evaluated Yap/Taz protein amount and nuclear localization as a readout (Dupont *et al.*, 2011). Treatment with C3 resulted in a significant decrease in YAP protein (on days 3 and 8) and TAZ protein (on days 1, 3, and 5; Supplemental Figure S3) and significantly decreased Yap nuclear localization on day 3 (Figure 1G and Supplemental Figure S4). As expected, given that the cells were on glass and maximally mechanoactivated, LPA treatment trended toward an increase, but did not significantly alter total YAP/TAZ protein amounts or its nuclear localization (Supplemental Figure S3 and Figure 1G). Taken together, these results support that the inverse relationship between elevated Rho signaling (mechanoactivation) and chondrogenic gene expression may be mediated by Yap.

To establish the direct role of Yap/Taz in antagonizing chondrogenic differentiation, ATDC5 cells were next transiently transfected with siRNA directed against *Yap1* (*Yap*) and *Wwtr1* (*Taz*) and assessed for chondrogenic gene expression 5 d posttransfection. Immunoblots for YAP/TAZ confirmed a significant decrease in both YAP and TAZ protein at this time point (Figure 2A). Likewise, qPCR for Yap and Taz target genes (Ccn1 and Ankrd1) showed a significant decrease in expression (Supplemental Figure S5). Interestingly, the single knockdown of either *Yap1* or *Taz* slightly increased chondrogenic marker

expression (Figure 2B) while simultaneous knockdown of both *Yap1* and *Taz* (Y/T) significantly increased chondrogenic marker expression. Lastly, to understand whether depleting Y/T absent of CM could drive chondrogenesis on its own, cells were transfected with siY/T in basal media (BM). In this nonchondrogenic context (BM), siY/T resulted in a significant increase in chondrogenic gene expression, reaching levels similar to that of CM Scrmbl control (Supplemental Figure S6). This finding supports the partial redundancy of Yap and Taz on chondrogenic gene expression, as has been reported for other differentiation processes, both in vitro and in vivo (Dupont *et al.*, 2011; Kegelman *et al.*, 2018) and further supports that Yap/Taz is a major regulator of chondrogenic differentiation.

To assess the effects of siY/T on the broader chondrogenic program, RNA-seq was performed. Similar to findings with C3 treatment, knockdown of Yap and Taz resulted in the significant up-regulation of a broad spectrum of chondrogenic genes, including *Gdf5*, *Col9*, and *Col11* (Figure 2C, i and ii). In addition, other genes important for articular cartilage function were also up-regulated, including the mechanosensitive ion channel *Trpv4* and pericellular matrix protein *Comp* (Figure 2C; Zaucke *et al.*, 2001; O'Conor *et al.*, 2014). GO analysis showed that siY/T regulated markers associated with cartilage development and chondrocyte differentiation (Figure 2C, iii). At the protein level, SOX9 and COLVI were also significantly increased (Figure 2D). Finally, to assess changes in cell morphology and actin cytoskeleton following si*Y/T*, cells were evaluated 4 d posttransfection and 1 d after transfer to glass at low density. Compared to controls, si*Y/T* cells had no detectable Yap staining, retained some actin stress fibers, and showed a significant reduction in both cell and nuclear area (Figure 2, E and F). Taken together, these data support that Yap/Taz acts to negatively regulate chondrogenic gene expression.

To elucidate whether knocking down Yap/Taz increased chondrogenic gene expression as a result of decreased Yap/Taz nuclear localization, cells were seeded on substrates whose stiffness more closely approximate soft tissues. This complementary model results in a scenario in which Yap/Taz nuclear localization is not at its maxima (as it is on glass). To achieve this, we used soft polyacrylamide (PA) hydrogels, substrates commonly used to assess how changes in substrate stiffness impact mechanotransduction. Cells were seeded at low density on PA gels of 5 or 55 kPa, values that are comparable to that of the articular chondrocyte pericellular matrix (Wilusz *et al.*, 2014). After 2 d, actin cytoskeletal architecture was assessed. Cells on 5 kPa gels were much smaller with punctate actin and few stress fibers observed (Figure 3A). On 55 kPa gels, actin stress fibers were present in greater abundance, though not as pronounced as on glass (Figure 3A). Additionally, cell and nuclear area were significantly smaller on 5 and 55 kPa compared with glass, with no significant difference between cells on 5 and 55 kPa (Figure 3B). Consistent with these changes in morphology, YAP nuclear localization also decreased on 5 and 55 kPa gels, compared with glass (Figure 3C). Based on these differences, we isolated cells from each of these conditions to assay for chondrogenic gene expression and protein abundance. Markers of chondrogenic differentiation all significantly increased on 5 kPa gels compared with glass, while cells on 55 kPa gels showed an intermediate level of chondrogenic gene expression (Figure 3D). Interestingly, immunoblots for YAP and TAZ showed a slight increase in total YAP protein in cells on 5 kPa gels compared with glass (Supplemental Figure S7). At the protein level, SOX9 and COLIV significantly increased on 5 kPa gels compared with glass (Figure 3E). Consistent with previous findings, these results demonstrate that decreasing substrate stiffness decreases YAP nuclear localization and increases chondrogenic gene expression (Allen *et al.*, 2012).

Next, to understand the role of changing substrate stiffness on the broader chondrogenic expression profile, RNA-seq was performed, comparing cells on glass to those on 5 and 55 kPa gels. Similar to both C3 treatment and si*Y/T*, cells on 5 and 55kPa gels showed increases in *Gdf5*, *Col6*, *Col9*, *Col11*, and *Trpv4* (Figure 3F; highlighted points in volcano plot, i, and heatmap, ii). Additionally, *Prg4*, an important lubricating glycoprotein in joints (Jay *et al.*, 2007; Maenohara *et al.*, 2021), was significantly increased on both 5 and 55 kPa gels (Figure 3F). Lastly, *Hspg2*, an important pericellular matrix protein (Wilusz *et al.*, 2012), was significantly up-regulated on 5 kPa gels (Figure 3F). We next performed GO analysis to identify pathways differentially regulated by soft substrates. This analysis revealed similar categories as identified in the YAP/TAZ knockdown studies, including ECM organization, cartilage development, and chondrocyte differentiation (Figure 3F, iii). These results further support that decreased mechanoactivation drives commitment to chondrogenesis.

To integrate these findings, we combined the RNA-seq information from the above perturbations into one data set. We found common pathways affected by these prochondrogenic perturbations (C3, siY/T, 5 kPa, 55 kPa) and plotted significant differentially expressed genes into Venn diagrams (Figure 4A, i–iii, Supplemental Figure S8A, i–iv, and Supplemental Material). Between these four groups, 27 genes were similarly up-regulated (Figure 4A, i). GO analysis revealed that these genes binned into categories relating to cartilage development, cartilage condensation, ossification, ECM organization, and chondrocyte differentiation (Figure 4A, ii). Of note, *Col2a1*, *Col9a2*, *Col11a1*, *Trpv4*, *Gdf5*, and *Sox6* were all significantly up-regulated (Figure 4A, iii). Next, we wanted to assess the relationships between both pro- and anti-chondrogenic perturbations using hierarchical clustering of genes binned in GO terms from Figure 4A, iii (Figure 4B, i–iv). Generally, LPA treatment (which increases cell mechanoactive state) resulted in an expression profile that was most dissimilar from all the other groups. Conversely, perturbations that decreased cell mechanoactive state (i.e., soft substates; siY/T, and C3 treatment of cells on glass) resulted in a broad induction of the chondrogenic program, with these groups most similar to one another. Interestingly, these prochondrogenic groups were not identical, with the 5 and 55 kPa groups more closely related to one another relative to either the siY/T- or C3-treated groups. These soft substrates also resulted in the largest increase in chondrogenic gene expression (*Col9*, *Col11*, *Sox6*, *Prg4*, and *Gdf5*) compared with the C3 and siY/T groups.

The above findings showed that elimination of YAP on glass promoted chondrogenesis (Figure 2), and that decreasing substrate stiffness promoted chondrogenesis (while decreasing YAP nuclear localization; Figure 3). To establish whether, in this more physiologic and softer microenvironmental context (where cells are not maximally mechanoactivated), Rho modulation through Yap nuclear localization is regulating chondrogenic gene expression, cells were seeded on PA gels in conjunction with Rho activation and/or inhibition. Specifically, cells were seeded on 55 kPa gels for 2 d and were treated with either C3 or LPA. C3 treatment on 55 kPa PA gels decreased cell size and actin stress fiber formation, resulting in cells resembling those on the softer 5 kPa gels (Figure 5A, and Supplemental Figure S9A, i). Conversely, cells on 55 kPa treated with LPA showed a more elongated morphology with more organized actin stress fibers, more akin to those on glass (Figure 5A, and Supplemental Figure S9S, i). Under these same conditions, C3 treatment significantly decreased YAP nuclear localization while LPA treatment increased YAP nuclear localization (Figure 5, A and B, and Supplemental Figure S9A, i). In keeping with this, C3 treatment on 55 kPa gels significantly increased

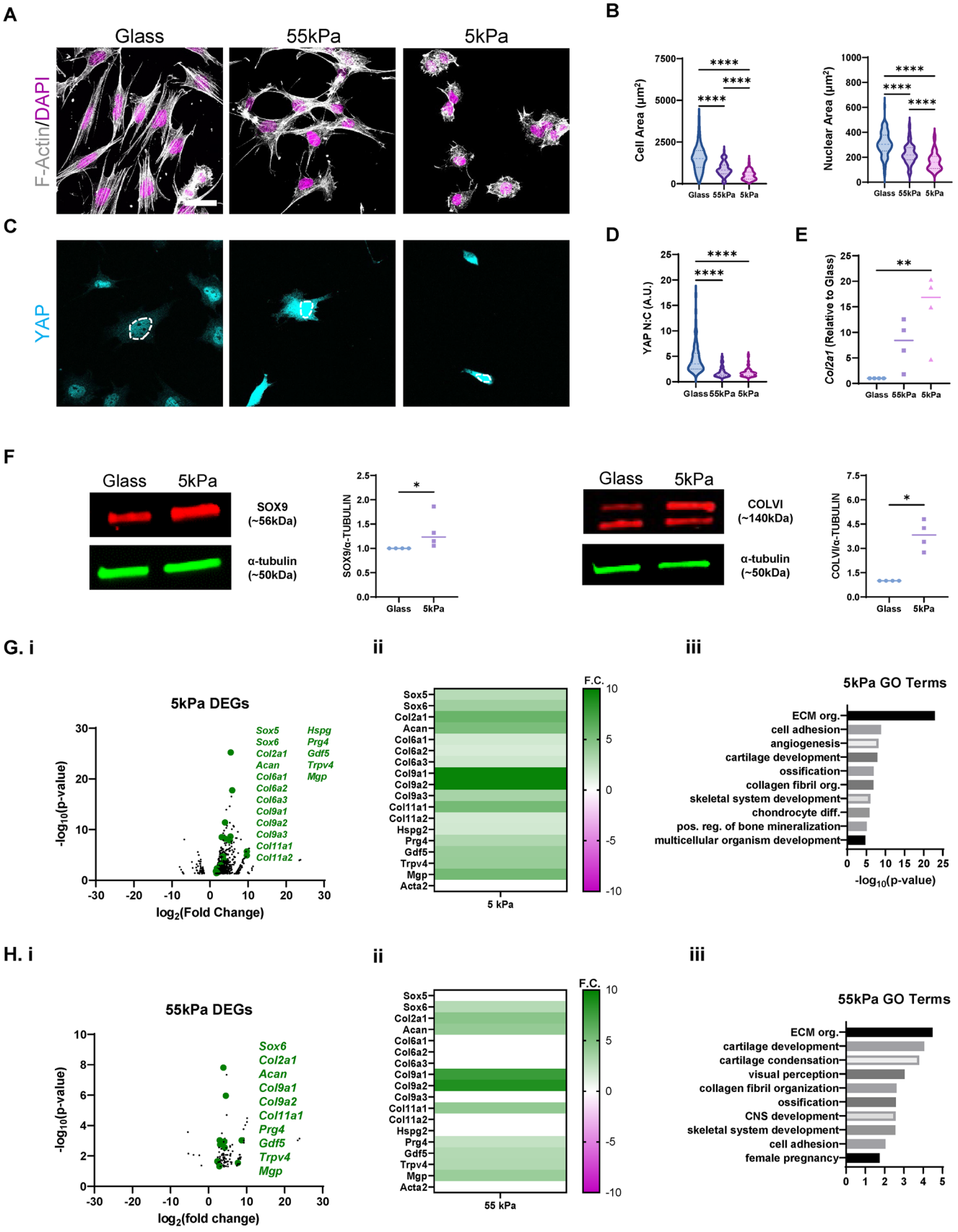

FIGURE 3: Rho modulates chondrogenic gene expression through Yap nuclear localization. (A) F-actin immunostaining of cells plated on PA gels and glass after 2 d in low-density culture in CM. Nuclei stained with DAPI. Maximum projection z-stack confocal images. $n = 3$ independent trials. Scale bar = 30 μm. (B) Quantification of cell and nuclear area on glass, and 5 and 55 kPa gels in CM. (C) Yap immunostaining of cells on glass and on 55 and 5 kPa PA gels after

chondrogenic gene expression, while LPA treatment significantly decreased chondrogenic gene expression (Figure 5C). These results indicate that, under conditions where Rho activity can be increased or decreased (on 55 kPa gels), these changes impact chondrogenic gene expression (negatively or positively) by regulating YAP nuclear localization.

Having defined this intermediate point, where chondrogenic state can be impacted in both directions by changes in mechanoactivation of cells, we next sought to determine whether Yap is central to this Rho-mediated chondrogenic response in this physiological context. To do so, cells were transfected with si*Y/T* and seeded 4 d posttransfection on 55 kPa gels for 1 additional day, in the presence or absence of LPA or C3. Within this context, siY/T significantly decreased Yap target gene expression (*Ccn1* and *Ankrd1*) indicating reduced Yap activity (Supplemental Figure S10). If Yap/Taz was essential for conveying mechanical information to impact chondrogenic state, then we would expect that Yap knockdown would block the effects of LPA in this context. Conversely, if other factors mediate the suppression of chondrogenesis with an increase in Rho signaling, then we would expect LPA to significantly decrease chondrogenesis in this context. Our findings show that the former is true, where si*Y/T* on 55 kPa gels significantly increased chondrogenic gene expression and this increased chondrogenesis was maintained even with the addition of LPA (Figure 5D). Lastly, to show that Rho inhibition is mediated primarily through Yap/Taz signaling, and not through other pathways sensitive to Rho inhibition, cells were transfected with siY/T and simultaneously treated with C3. Here, if Yap/Taz signaling were the primary mediator, we would expect no further elevation of chondrogenesis with Rho inhibition. Indeed, Rho inhibition in cells depleted of Yap and Taz did not result in any further increases in chondrogenic gene expression (Figure 5E). Taken together, these results support the hypothesis that decreasing the mechanoactive state of chondrocytes by lowering Rho activity inhibits YAP nuclear localization and this in turn allows for a chondrogenic program to be initiated and sustained.

DISCUSSION

This study expands our knowledge regarding how mechanical regulation of chondrogenic gene expression is mediated by Yap/Taz. We show, in multiple contexts using both direct (siY/T) and indirect (C3 and decreased substrate stiffness) perturbations, that a decrease in the mechanoactive state of cells (cell and nuclear area, actin stress fibers, and Yap/Taz nuclear localization) results in a convergence toward a similar chondrogenic program. This convergence is highlighted by Venn diagrams showing the substantial overlap in differentially expressed genes across the various pro-chondrogenic perturbations used in this study (Figure 4A and Supplemental Figure S8). These and other identified genes provide insight into the intersection of microenvironmental cues and key pathways involved in the mechanoregulation of chondrogenic differentiation.

The above data firmly establish that mechanical inputs regulate chondrocyte phenotype and operate through a Rho-mediated signaling mechanism. However, it remained unclear precisely how this mechanical signaling was relayed to regulate phenotype. Our results showed that decreasing Yap/Taz amount or nuclear localization either directly (siY/T) or indirectly (C3 and soft substrates) increased canonical chondrogenic gene expression, suggesting that Yap might be a key player. Importantly, when cells were placed on intermediate stiffness substrates with Yap/Taz depletion, LPA treatment did not significantly decrease chondrogenic gene expression. Likewise, when Yap/Taz was depleted along with further inhibition of Rho signaling (with C3), no additional increase in chondrogenic expression was observed. While we cannot rule out other possible effects of Yap and/or Taz in the cytosol, these data do support the hypothesis that elevated Rho signaling decreases chondrogenic gene expression by increasing Yap/Taz nuclear localization, and that mobilization of these transcriptional coactivators is necessary and sufficient for the suppression of the chondrogenic phenotype.

How exactly nuclear Yap/Taz suppresses chondrogenesis remains an open question (Figure 6). Yap may act as a direct transcriptional corepressor of chondrogenesis by binding to a TEAD binding site on the *Sox9* promoter itself (Goto *et al.*, 2018) or by binding to (and blocking transcription at) Sox9 target genes. Alternatively, Yap may act as a transcriptional coactivator at anti-chondrogenic loci (e.g., promoting expression of factors involved in cell spreading and force generation; Nardone *et al.*, 2017; Mason *et al.*, 2019) with increased mechanoactivation. Importantly, Taz may also play an important role in modulating the ability of Yap to regulate chondrogenic differentiation. For example, Taz can regulate the ability of Yap to promote or inhibit osteogenic differentiation, and does so in a Runx2-dependent manner (Byun *et al.*, 2014; Kegelman *et al.*, 2018). Our data show that depleting both Yap and Taz was necessary to robustly increase chondrogenic gene expression, supporting that both are necessary but not individually sufficient to regulate chondrogenic differentiation (Figure 2B). Interestingly, in skeletal progenitors, Sox9 and Runx2 have opposing roles in regulating cell fate, where Sox9-dominant cells persist as chondrocytes while Runx2-dominant cells become osteocytes (Eames *et al.*, 2004). Similarly, during limb development, cells in the cartilage anlage show low nuclear Yap and increased p-Yap while hypertrophic/terminal chondrocytes show the opposite (Karystinou *et al.*, 2015). Integrating these points, it is possible that Yap/Taz may act as a mechanomodulator during limb development, specifying which cells become chondrocytes (low nuclear Yap/Taz, low Rho, low mechanoactivation) and which progress toward hypertrophic phenotypes (Figure 5C). Future experiments, involving ChIPseq for both Sox9 and Yap under changing mechanobiologic conditions, will be required to

2 d in culture with CM. $n = 3$ independent trials. Maximum projection z-stack confocal images. Scale bar = 30 μm. Nuclei are outlined in white. (D) Quantification of YAP nuclear:cytoplasmic ratios (YAP N:C). $n = 3$ replicates, 20–30 cells per group/per replicate. (E) *Col2a1* gene expression of cells on glass, and 5 and 55 kPa PA gels after 2 d of culture in CM. $n = 4$ independent trials. (F) Left, SOX9 and COLVI immunoblot after 2 d of low-density culture on glass, and 5 kPa in CM. Right, quantification of fold change in protein. $n = 5$ independent trials. α-Tubulin was used as a loading control. (G, i) Volcano plot showing differentially expressed genes (DEGs) in cells on 5 kPa gels in CM, compared with glass. Genes with significant differences (chartreuse and magenta dots) in expression that have an established role in chondrocyte differentiation or disease. (G, ii) Heatmap of noted genes in i. (G, iii) Bar graphs showing gene ontology groups identified from DEGs in i, in descending order of significance. $n = 2$ independent trials. (H, i) Volcano plot showing DEGs of cells on 55 kPa gels in CM, compared with glass. (H, ii) Heatmap of noted genes in i. (H, iii) Bar graphs showing gene ontology groups identified from DEGs in H, i, in descending order of significance. $n = 2$ independent trials (*, $p < 0.05$; **, $p < 0.01$; ****, $p < 0.0001$.

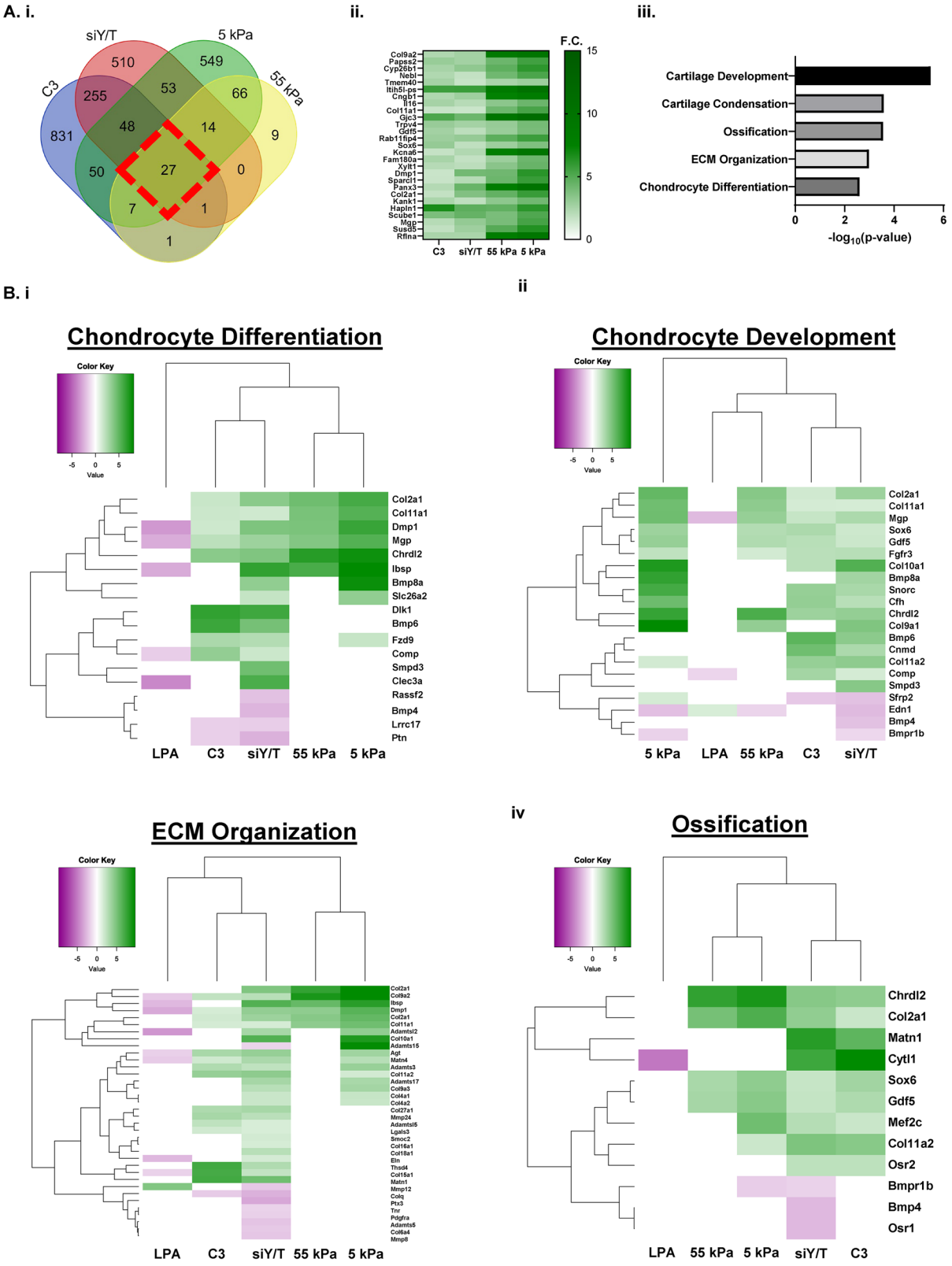

FIGURE 4: Integration of RNA-seq data sets identifies pathways regulated by prochondrogenic modulators. (A, i) Venn diagrams integrating differentially regulated genes in response to prochondrogenic modulators. (A, ii) Heatmap showing change in expression of genes common to all prochondrogenic modulators (red dotted box in i). (A, iii) GO terms resulting from analysis of the common 27 genes set. (B) Hierarchical clustering heatmaps from RNA-seq data for differentially expressed genes in the GO terms: (B, i) Chondrocyte Differentiation, (B, ii) Cartilage Development, (B, iii) ECM Organization, and (B, iv) Ossification. Cyan indicates down-regulated, magenta indicates up-regulated, and white indicates no change in expression compared with glass/plastic control for each group. Cartilage Condensation cluster not shown given that all but two genes were included in other clusters.

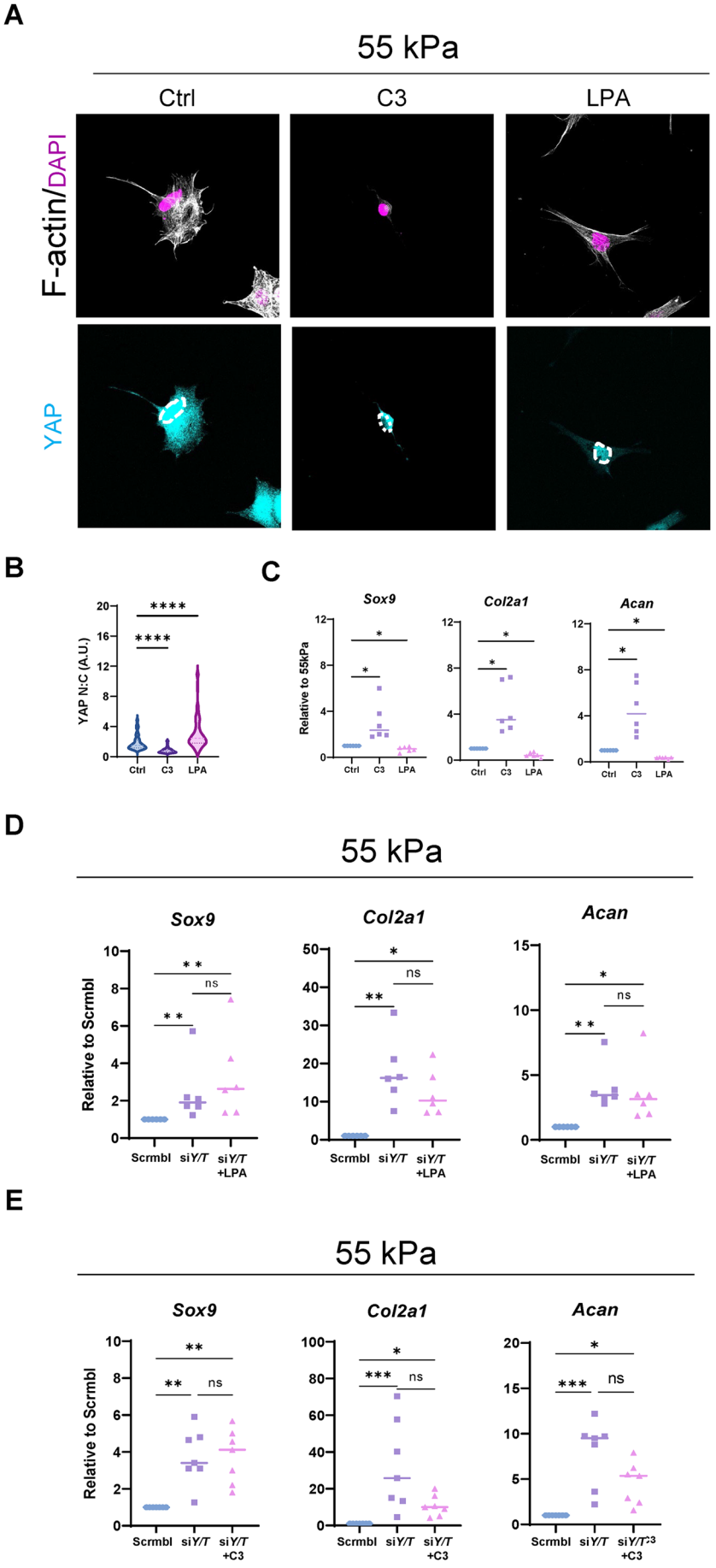

establish the precise location and mechanism by which mechanoactive Yap/Taz regulates chondrogenic differentiation through altered Yap/Taz–chromatin interactions.

Taken together, our data provide new insight into mechanical regulation of the chondrocyte phenotype that may be leveraged to promote therapeutic cell expansion and design improved regenerative strategies. Specifically, given the growing number of small molecule modulators of Rho and Yap/Taz that are available, as well as biomaterials that can regulate these pathways, future culture conditions may be designed to specifically bias cells toward a chondrogenic phenotype. Such advances could be critically important for maintaining chondrocyte identity before therapeutic applications in restoring damaged or diseased articular cartilage.

MATERIALS AND METHODS

Request a protocol through *Bio-protocol*.

Cell culture

ATDC5 cells were cultured in a 1:1 Dulbecco's modified Eagle's medium (Life Technologies; 12430047) and Ham's F-12 medium (Corning; MT10-080-CV) supplemented with 5% fetal bovine serum (BioTechne; S11150) and 1% penicillin/streptomycin and fungizone (Life Technologies; 15240062). Cells were cultured at 37°C under 5% CO_2. To differentiate ATDC5 cells toward a chondrogenic lineage, chemically defined media including TGF-β3 (10 ng/ml; R&D Systems; DY243) was applied, as described previously (Huang *et al.*, 2008). For monolayer experiments, cells were seeded at high density in either 24-well plates for RNA extraction (at 105,000 cells/cm^2) or in 6-well plates (at 83,333 cells/cm^2). Cells tested negative for mycoplasma using the Invivogen Mycostrip test kit (rep-mys-10).

Transfection

ATDC5 cells were transiently transfected with 5 pmol of SMARTPOOL ON-TARGETplus siRNA to *Yap1*

FIGURE 5: Rho acts through YAP to negatively regulate chondrogenic gene expression. (A) F-actin and Yap immunostaining of cells on 55 kPa gels treated with C3 or LPA in CM. Nuclei stained with DAPI. Scale bar = 30 μm. Maximum projection z-stack confocal images. $n = 3$ independent trials. Nuclei are outlined in white for YAP panels. (B) Quantification of YAP nuclear:cytoplasmic ratios (YAP N:C, right). $n = 3$ replicates, 20–30 cells per group/per replicate. (C) Chondrogenic gene expression of cells seeded on 55 kPa gels for 2 d with or without C3 or LPA treatment in CM. (D) Chondrogenic gene expression of cells 4 d after transfection with si*Y/T*, and 1 d after reseeding on 55 kPa gels and treatment with LPA in CM. $n = 6$ independent trials. (E) Chondrogenic gene expression of cells 4 d after transfection with si*Y/T*, and 1 d after reseeding on 55 kPa gels and treatment with C3 in CM. $n = 6$ independent trials. *, $p < 0.05$; **, $p < 0.01$; ***, $p < 0.001$; ****, $p < 0.0001$.

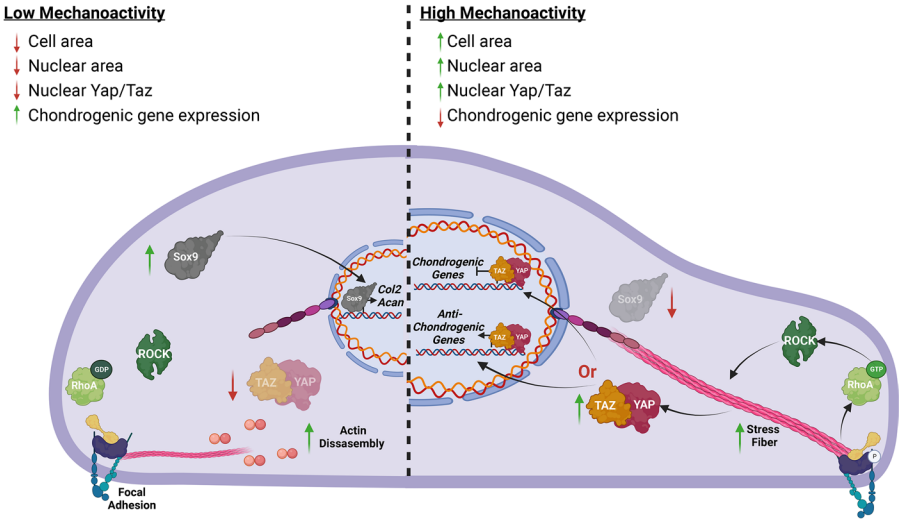

FIGURE 6: A model of mechanoregulation of chondrogenesis. Model depicting how low mechanoactivity (left) decreases Yap/Taz protein and nuclear localization, allowing Sox9 to positively regulate chondrogenic gene expression. Right, chondrocytes experiencing high mechanoactivity promote Yap/Taz nuclear localization via elevated Rho signaling to repress chondrogenic gene expression and/or promote expression of anti-chondrogenic factors.

and *Wwtr1* (2.5 pmol each for double knockdown studies) or a nontargeting control (Dharmacon) using lipofectamine RNAiMAX according to the manufacturer's instructions. The transfection cocktail was placed onto the tissue culture plate before adding cells (52,632 cells/cm^2). Media was changed 3 d posttransfection and cells were collected 5 d posttransfection for analysis.

PA gel fabrication

PA hydrogels were prepared as described previously (Haupt *et al.*, 2019). Briefly, 167 or 500 µl of 37.5:1 acrylamide:bis-acrylamide (Biorad; 1610158) was diluted in 833 or 500 µl of MilliQ H_2O to generate hydrogels with a stiffness of 5 or 55 kPa, respectively. Gels (55 µl) were polymerized under glass coverslips via addition of 0.2% TEMED (BioRad; 1610800) and 10% APS (BioRad; 1610700). After polymerization, gels were activated with 2 mg/ml sulfo-SANPAH (Pierce Protein Biology/Life Technologies; 22589) and then coated with fibronectin (20 mg/ml; Sigma Aldrich; F1141) for 45 min at room temperature. Glass conditions were also coated in fibronectin to keep consistent adhesive ligands. Gels were sterilized under UV in a tissue culture hood before cell seeding. Cells were seeded at 100,000 cells per glass slide.

Pharmacological regulation of RhoA activity

To inhibit Rho activity, C3 (Cytoskeleton; CT04-A) was applied at 0.3 mg/ml while Rho activation was achieved via oleoyl-L-α-lysophosphatidic acid sodium salt (LPA; Sigma L7260) applied at 50 mM (for monolayer experiments) or 20 mM (for PA gel studies). Small molecules were added 2 h postseeding and replaced every day of culture with complete media changes.

RNA isolation, cDNA synthesis, and qRT-PCR

ATDC5 cells were collected at defined time points by releasing cells from the surface with trypsin (Life Technologies; 25200056; for monolayer experiments) or Tryp-LE (Life Technologies; 12605036; for PA gel studies). Cells were pelleted at 300 × *g* for 5 min and frozen at –80°C before RNA isolation. RNA was isolated using the Directzol kit with DNAse I treatment (Zymo Research; R2050). cDNA was synthesized using the SuperScript VILO IV kit (Invitrogen; 11756050). Quantitative RT-PCR was run on a Quantstudio 6 Pro using Fast SYBR reagents (ThermoFisher; 4385618) for 40 cycles with custom-designed primers (see Supplemental Table S1 for primer sequences). 18S was used as a housekeeping gene for all experiments and fold changes were calculated using the double delta Ct method. Experimental conditions for each independent trial were normalized to their respective control group.

Immunofluorescence staining and imaging

At the indicated time points, cells were fixed in 4% paraformaldehyde for 20 min at room temperature and then washed three times with phosphate-buffered saline (PBS). Cells were then permeabilized with 0.3% Triton X-100 (Sigma; T8787) in PBS for 5 min at room temperature. Cells were then washed three times with PBS and then place in blocking buffer (3% BSA; Sigma; A9418; in PBS) for 1 h at room temperature. All antibodies were diluted in blocking buffer. Primary antibodies (Collagen VI, rabbit; Abcam; 6588, 1:250; YAP, rabbit; Cell Signaling; #14074; 1:500) were incubated overnight at 4°C, and were washed three times with PBS before secondary antibody incubation. Filamentous actin was visualized using Alexa Fluor 555–conjugated phalloidin during the secondary antibody step; this agent was incubated for 1 h at room temperature in the dark along with other Alexa Fluor antibodies used to indirectly visualize primary antibody targets. Coverslips and/or PA gels were mounted with ProLong Gold with DAPI (Invitrogen; P36934).

For YAP nuclear to cytoplasmic staining and analysis, average staining intensity within the nucleus and within the cytoplasm was quantified using ImageJ (National Institutes of Health, Bethesda, MD); these intensities were used to calculate a nuclear/cytoplasmic YAP ratio (Driscoll *et al.*, 2015). ATDC5 cells were imaged at room temperature on a Nikon A1R confocal microscope using NIS-Elements software with 20×, 40×, and 63× objectives. Confocal z stacks were converted to maximum projections for analysis and display.

Immunoblotting

For monolayer experiments, cells were washed once in cold PBS and then lysed in RIPA buffer (supplemented with protease inhibitors and phosphatase inhibitors; Thermo; 78441) for 30 min on ice. During incubation, the whole cell lysate (WCL) was pipetted vigorously to break up the lysate. WCL was centrifuged at 13,400 × *g* for 15 min at 4°C and the supernatant was collected for quantification and immunoblotting.

Before immunoblotting, WCL was quantified using the bicinchoninic acid assay, with bovine serum albumin used as a standard. WCL was denatured and reduced using 4X Li-COR sample buffer (Li-COR Biosciences; 928-40004) with β-mercaptoethanol and boiling at 95°C for 5 min. A total of 25 µg of protein was loaded per lane in Tris-glycine gels (BioRad; 4568084) under denaturing conditions. Gels were run for 40 min at a constant voltage of 150 V. Protein was transferred to a nitrocellulose membrane using the TransBlot Turbo transfer system (BioRad; 1704150) and equal transfer was qualitatively determined using Ponceau S stain. Membranes were then

blocked in Intercept TBS blocking buffer (Li-COR; 927-60001) for 1 h at room temperature with gentle rocking. Primary antibodies were diluted in a 1:1 solution of Intercept TBS blocking buffer and 0.1% TBS-Tween-20 (TBS-T). Primary antibodies (Sox9, rabbit; Cell Signaling; #82630; 1:500; α-tubulin, mouse; Sigma; #T5168; 1:1000; Collagen VI, rabbit; Abcam; 6588; 1:250; YAP, rabbit; Cell Signaling; #14074; 1:500; YAP/TAZ, rabbit; Cell Signaling; #93622; 1:1000; α-tubulin; Abcam; rabbit; #18251; 1:1000; p-YAP (Ser 127); Cell Signaling; rabbit; #13008; 1:1000) were incubated overnight at 4°C with gentle rocking. Membranes were washed three times with TBS-T for 5 min with gentle rocking. Secondary antibodies were also diluted in Intercept TBS blocking buffer: TBS-T for 1 h at room temperature in the dark with gentle rocking. Finally, membranes were washed three times with TBS-T for 5 min with gentle rocking.

To visualize protein levels, an Odyssey Infrared Imaging System (Li-COR Biosciences; model 9120) was used. To measure differences in protein levels between groups, images were analyzed in Fiji using the average fluorescent intensity of bands of the same area normalized to α-tubulin. Fold changes were calculated using normalized fluorescent intensity and control samples as a reference (Control, Scrmbl, or Glass). Experimental conditions for each independent trial were normalized to their respective control group.

Cell and nuclear area

Cytoskeletal architecture was visualized as described above using immunofluorescence, and epifluorescent images were captured on a Zeiss Axio Observer microscope at 20× magnification. Cell Profiler was used to calculate cell area, nuclear aspect ratio, and nuclear area as described in McQuin *et al.* (2018). Outliers for multicellular aggregates were manually removed and confirmed using the ROUT outlier test.

RNA-seq and analysis

A total of 1 µg of RNA was analyzed and sequenced by the University of Pennsylvania Children's Hospital of Philadelphia Center for Applied Genomics core. Briefly, RNA integrity number was assessed by the Agilent Tapestation system. Each RNA sample used in RNA-seq had an RNA integrity number score above 9. Samples were then prepped for sequencing using TruSeq Stranded mRNA Library Prep and sequenced on a Novaseq 6000. After sequencing, the resulting paired end reads were aligned to the reference genome mm10 using hisat2 (Zhang *et al.*, 2021). Aligned sam files were then converted to bam files using Picard SortSam ("Picard Toolkit." 2019. Broad Institute, GitHub Repository. https://broadinstitute.github.io/picard/). Count matrices were generated using FeatureCount. Deseq2 was used for differential expression analysis (Love *et al.*, 2014). To annotate all expressed genes, the Entrez gene ID was converted to the common gene name. Volcano plots were generated using Prism to visualize differentially expressed genes with a fold change cutoff of greater/less than or equal to 1.5/–1.5 and $-\log_{10} p$ values of greater than or equal to 1.3. Venn diagrams of significant differentially expressed genes from all RNA-seq data sets were generated using https://bioinformatics.psb.ugent.be/webtools/Venn/. A list of differentially expressed genes between groups diagrammed in Figure 4 and Supplemental Figure 8 is provided in the Supplemental Material.

Statistical analysis

For qPCR and immunoblotting results with three groups, a nonparametric one-way ANOVA (Kruskall-Wallace) with an uncorrected Dunn's test was used. For immunoblotting results with two groups (Figure 3) a nonparametric *t* test (Mann-Whitney) was used. For cell/nuclear area quantification a parametric one-way ANOVA was used. For Yap nuclear:cytoplasmic ratio experiments, a parametric one-way ANOVA with Brown-Forscythe correction was used.

ACKNOWLEDGMENTS

This work was supported by a Gilliam Fellowship from the Howard Hughes Medical Institute. Additional support was provided by the National Institutes of Health (Grants no. R01 AR-071399, no. R01 AR-079224, and no. R01 AR-077362) and the NSF Science and Technology Center for Engineering Mechanobiology (CMMI-1548571). ATDC5 cells were a gift from Veronique Lefebvre's lab at the Children's Hospital of University of Pennsylvania. Figure 5B was created with Biorender.com. Raw and Processed RNA-seq data files are available on GEO at GEO Accession number GSE231925

REFERENCES

Allen JL, Cooke ME, Alliston T (2012). ECM stiffness primes the TGFβ pathway to promote chondrocyte differentiation. Mol Biol Cell 23, 3731–3742.

Barna M, Niswander L (2007). Visualization of cartilage formation: insight into cellular properties of skeletal progenitors and chondrodysplasia syndromes. Dev Cell 12, 931–941.

Blain EJ (2009). Involvement of the cytoskeletal elements in articular cartilage homeostasis and pathology. Int J Exp Pathol 90, 1–15.

Byun MR, Sung MK, Kim AR, Lee CH, Jang EJ, Jeong MG, Noh M, Hwang ES, Hong J-H (2014). (–)-Epicatechin gallate (ECG) stimulates osteoblast differentiation via Runt-related transcription factor 2 (RUNX2) and transcriptional coactivator with PDZ-binding motif (TAZ)-mediated transcriptional activation. J Biol Chem 289, 9926–9935.

Caliari SR, Vega SL, Kwon M, Soulas EM, Burdick JA (2016). Dimensionality and spreading influence MSC YAP/TAZ signaling in hydrogel environments. Biomaterials 103, 314–323.

Carley E, Stewart RM, Zieman A, Jalilian I, King DE, Zubek A, Lin S, Horsley V, King MC (2021). The LINC complex transmits integrin-dependent tension to the nuclear lamina and represses epidermal differentiation. eLife 10, e58541.

Das A, Fischer RS, Pan D, Waterman CM (2016). YAP nuclear localization in the absence of cell-cell contact is mediated by a filamentous actin-dependent, myosin II- and phospho-YAP-independent pathway during extracellular matrix mechanosensing. J Biol Chem 291, 6096–6110.

Decker RS, Um H-B, Dyment NA, Cottingham N, Usami Y, Enomoto-Iwamoto M, Kronenberg MS, Maye P, Rowe DW, Koyama E, Pacifici M (2017). Cell origin, volume and arrangement are drivers of articular cartilage formation, morphogenesis and response to injury in mouse limbs. Dev Biol 426, 56–68.

Deng Y, Wu A, Li P, Li G, Qin L, Song H, Mak KK (2016). Yap1 regulates multiple steps of chondrocyte differentiation during skeletal development and bone repair. Cell Rep 14, 2224–2237.

Driscoll TP, Cosgrove BD, Heo S-J, Shurden ZE, Mauck RL (2015). Cytoskeletal to nuclear strain transfer regulates YAP signaling in mesenchymal stem cells. Biophys J 108, 2783–2793.

Dupont S, Morsut L, Aragona M, Enzo E, Giulitti S, Cordenonsi M, Zanconato F, Le Digabel J, Forcato M, Bicciato S, *et al.* (2011). Role of YAP/TAZ in mechanotransduction. Nature 474, 179–183.

Eames BF, Sharpe PT, Helms JA (2004). Hierarchy revealed in the specification of three skeletal fates by Sox9 and Runx2. Dev Biol 274, 188–200.

Elosegui-Artola A, Andreu I, Beedle AEM, Lezamiz A, Uroz M, Kosmalska AJ, Oria R, Kechagia JZ, Rico-Lastres P, Le Roux A-L, *et al.* (2017). Force triggers YAP nuclear entry by regulating transport across nuclear pores. Cell 171, 1397–1410.e14.

Gao L, McBeath R, Chen CS (2010). Stem cell shape regulates a chondrogenic versus myogenic fate through Rac1 and N-cadherin. Stem Cells 28, 564–572.

Goto H, Nishio M, To Y, Oishi T, Miyachi Y, Maehama T, Nishina H, Akiyama H, Mak TW, Makii Y, *et al.* (2018). Loss of *Mob1a/b* in mice results in chondrodysplasia due to YAP1/TAZ-TEADs-dependent repression of SOX9. Development 145, dev.159244.

Haupt J, Stanley A, McLeod CM, Cosgrove BD, Culbert AL, Wang L, Mourkioti F, Mauck RL, Shore EM (2019). ACVR1R206H FOP mutation alters mechanosensing and tissue stiffness during heterotopic ossification. Mol Biol Cell 30, 17–29.

Heo S-J, Thorpe SD, Driscoll TP, Duncan RL, Lee DA, Mauck RL (2015). Biophysical regulation of chromatin architecture instills a mechanical memory in mesenchymal stem cells. Sci Rep 5, 16895.

Huang AH, Yeger-McKeever M, Stein A, Mauck RL (2008). Tensile properties of engineered cartilage formed from chondrocyte- and MSC-laden hydrogels. Osteoarthritis Cartilage 16, 1074–1082.
Jay GD, Torres JR, Warman ML, Laderer MC, Breuer KS (2007). The role of lubricin in the mechanical behavior of synovial fluid. Proc Natl Acad Sci USA 104, 6194–6199.
Karystinou A, Roelofs AJ, Neve A, Cantatore FP, Wackerhage H, De Bari C (2015). Yes-associated protein (YAP) is a negative regulator of chondrogenesis in mesenchymal stem cells. Arthritis Res Ther 17, 147.
Kegelman CD, Mason DE, Dawahare JH, Horan DJ, Vigil GD, Howard SS, Robling AG, Bellido TM, Boerckel JD (2018). Skeletal cell YAP and TAZ combinatorially promote bone development. FASEB J 32, 2706–2721.
Koyama E, Shibukawa Y, Nagayama M, Sugito H, Young B, Yuasa T, Okabe T, Ochiai T, Kamiya N, Rountree RB, *et al.* (2008). A distinct cohort of progenitor cells participates in synovial joint and articular cartilage formation during mouse limb skeletogenesis. Dev Biol 316, 62–73.
Kumar D, Lassar AB (2009). The transcriptional activity of Sox9 in chondrocytes is regulated by RhoA signaling and actin polymerization. Mol Cell Biol 29, 4262–4273.
Love MI, Huber W, Anders S (2014). Moderated estimation of fold change and dispersion for RNA-seq data with DESeq2. Genome Biol 15, 550.
Luxton GWG, Gomes ER, Folker ES, Worman H, Gundersen GG (2011). TAN lines: A novel nuclear envelope structure involved in nuclear positioning. Nucleus 2, 173–181.
Maenohara Y, Chijimatsu R, Tachibana N, Uehara K, Xuan F, Mori D, Murahashi Y, Nakamoto H, Oichi T, Chang SH, *et al.* (2021). Lubricin contributes to homeostasis of articular cartilage by modulating differentiation of superficial zone cells. J Bone Miner Res 36, 792–802.
Mason DE, Collins JM, Dawahare JH, Nguyen TD, Lin Y, Voytik-Harbin SL, Zorlutuna P, Yoder MC, Boerckel JD (2019). YAP and TAZ limit cytoskeletal and focal adhesion maturation to enable persistent cell motility. J Cell Biol 218, 1369–1389.
McQuin C, Goodman A, Chernyshev V, Kamentsky L, Cimini BA, Karhohs KW, Doan M, Ding L, Rafelski SM, Thirstrup D, *et al.* (2018). CellProfiler 3.0: next-generation image processing for biology. PLoS Biol 16, e2005970.
Mehana E-SE, Khafaga AF, El-Blehi SS (2019). The role of matrix metalloproteinases in osteoarthritis pathogenesis: an updated review. Life Sci 234, 116786.
Nardone G, Oliver-De La Cruz J, Vrbsky J, Martini C, Pribyl J, Skládal P, Pešl M, Caluori G, Pagliari S, Martino F, *et al.* (2017). YAP regulates cell mechanics by controlling focal adhesion assembly. Nat Commun 8, 15321.
O'Conor CJ, Leddy HA, Benefield HC, Liedtke WB, Guilak F (2014). TRPV4-mediated mechanotransduction regulates the metabolic response of chondrocytes to dynamic loading. Proc Natl Acad Sci USA 111, 1316–1321.
Öztürk E, Despot-Slade E, Pichler M, Zenobi-Wong M (2017). RhoA activation and nuclearization marks loss of chondrocyte phenotype in crosstalk with Wnt pathway. Exp Cell Res 360, 113–124.
Ray P, Chapman SC (2015). Cytoskeletal reorganization drives mesenchymal condensation and regulates downstream molecular signaling. PLoS One 10, e0134702.
Sanchez-Adams J, Leddy HA, McNulty AL, O'Conor CJ, Guilak F (2014). The mechanobiology of articular cartilage: bearing the burden of osteoarthritis. Curr Rheumatol Rep 16, 451.
Sophia Fox AJ, Bedi A, Rodeo SA (2009). The basic science of articular cartilage: structure, composition, and function. Sports Health 1, 461–468.
Vanyai HK, Prin F, Guillermin O, Marzook B, Boeing S, Howson A, Saunders RE, Snoeks T, Howell M, Mohun TJ, Thompson B (2020). Control of skeletal morphogenesis by the Hippo-YAP/TAZ pathway. Development 147, dev.187187.
Wilusz RE, DeFrate LE, Guilak F (2012). A biomechanical role for perlecan in the pericellular matrix of articular cartilage. Matrix Biol 31, 320–327.
Wilusz RE, Sanchez-Adams J, Guilak F (2014). The structure and function of the pericellular matrix of articular cartilage. Matrix Biol J Int Soc Matrix Biol 39, 25–32.
Woods A, Wang G, Beier F (2005). RhoA/ROCK signaling regulates Sox9 expression and actin organization during chondrogenesis. J Biol Chem 280, 11626–11634.
Xu B, Song G, Ju Y, Li X, Song Y, Watanabe S (2012). RhoA/ROCK, cytoskeletal dynamics, and focal adhesion kinase are required for mechanical stretch-induced tenogenic differentiation of human mesenchymal stem cells. J Cell Physiol 227, 2722–2729.
Zaucke F, Dinser R, Maurer P, Paulsson M (2001). Cartilage oligomeric matrix protein (COMP) and collagen IX are sensitive markers for the differentiation state of articular primary chondrocytes. Biochem J 358, 17–24.
Zelenski NA, Leddy HA, Sanchez-Adams J, Zhang J, Bonaldo P, Liedtke W, Guilak F (2015). Type VI collagen regulates pericellular matrix properties, chondrocyte swelling, and mechanotransduction in mouse articular cartilage. Arthritis Rheumatol 67, 1286–1294.
Zhang Y, Park C, Bennett C, Thornton M, Kim D (2021). Rapid and accurate alignment of nucleotide conversion sequencing reads with HISAT-3N. Genome Res 31, 1290–1295.